Electric field-induced aging phase transformation in Al–Zn–Mg–Cu alloys: a first-principles study

Chun-mei Li[1,a], Nan-pu Cheng[1,b,*], Zhi-qian Chen[1,c], Xiao Li[1,d], Zhong-jing Xie[1,e] and Hong He

1 Faculty of Materials and Energy, Southwest University, Chongqing 400715, China

[a]lcm1998@swu.edu.cn, [b]cheng_np@swu.edu.cn, [c]chen_zq@swu.edu.cn, [d]lx123ppp@swu.edu.cn, [e]xzjlms13@swu.edu.cn

Keywords: Aging phase transformation, Electric field, First-principles, Al–Zn–Mg–Cu alloys

Abstract. The effect of electric fields on the aging phase transformation of Al–Zn–Mg–Cu alloys is investigated with the first-principles method combined with vacancy mechanism. The effects of external electric intensity on aging phase transformation are analyzed. Results show that during aging in an applied electric field lower than 26MV/cm, phase transformation from the GP zones to η' will be accelerated while the phase transformation from η' to η phase will be delayed.

Introduction

The electric field, as a special energy field, has garnered significant attention from scholars [1-2] because of its special effects on the preparation and heat treatment of metals and alloys. Wang et al. [3] concluded that electric pulse modification of liquid metal led to a more homogeneous phase distribution and was beneficial to grain refinement. And Liu et al. [4] stated that electric field applied during solution treatment induced larger subgrain and increased volume fraction of precipitates, which resulted in higher ductility. All these experimental results show that applying an external electric field is an effective way to control the microstructure and improve their properties. However, the influence of an electric field on thermodynamic properties has not got much attention [5].

In this study, the phase transformations of Al–Zn–Mg–Cu alloys during aging treatment with and without an external electric field are discussed by first-principles Gibbs energy calculations. Zhang et al. [5] has investigated phase transformations with an electric field by calculating the Gibbs free energy of atom clusters in an Al–Cu–Li alloy. Also the first-principles method has been successfully utilized to analyze the transformation of the theta phase in Mg–Li–Al alloys [6], and the effect of external electric field on single-walled nanotube [7]. However, Zhang et al.'s study mainly focused on horizontal comparison based on substitution of atoms. In the present study, the thermodynamic properties of the precipitates, namely GPI, GPII, metastable η' phase and stable η phase, during aging in Al–Zn–Mg–Cu alloys are constructed and calculated.

Theory and methodology

The binding energies of the GP zones, metastable η' phase and the stable η phase are calculated with

* Corresponding author.
E-mail address: lcm1998@swu.edu.cn

the first-principles method, which is based on the density functional theory (DFT) plane-wave method [8]. The plane-wave pseudopotential total energy calculation [9] is performed with the CASTEP [10] and Dmol3 [11] modules of Materials Studio.

The results of vibrational analysis or Hessian evaluation [12] have been utilized to compute enthalpy (H), entropy (S), and free energy (G) as functions of temperature. The absolute value of the energies at 0K is meaningless for the analysis of the effect of external electric field. Instead, the change of the relative value of energy is significant, so in the study of this paper the energy at 0K is counted as zero. The various translational, rotational, and vibrational components are utilized to calculate H, S, G at finite temperatures as discussed below [13]. Two expressions are provided in each case for rotational contributions: one for linear system, and the other for nonlinear system.

Enthalpy correction H is provided by

$$H(T) = E_{\text{vib}}(T) + E_{\text{rot}}(T) + E_{\text{trans}}(T) + RT \tag{1}$$

where the subscripts represent the vibrational, rotational, and translational contributions, and R is the ideal gas constant. The contributions are provided by

$$E_{\text{trans}} = 3RT/2 \qquad (\text{for} \quad Q_{\text{trans}} = \sum_i \frac{\sqrt{2pMkT/N_{\text{a}}}}{h}) \tag{2}$$

$$E_{\text{rot}}(linear) = RT \quad (\text{for} \quad Q_{\text{rot}}(linear) = \frac{8p^2IkT}{sh^2}) \tag{3}$$

$$E_{\text{rot}}(nonlinear) = 3RT/2 \qquad (\text{for} \quad Q_{\text{rot}}(nonlinear) = (\frac{\sqrt{p}}{s})[\frac{8p^2kT}{h^2}]^{3/2}\sqrt{I_{\text{A}}I_{\text{B}}I_{\text{C}}}) \tag{4}$$

$$E_{\text{vib}} = \frac{R}{k}\frac{1}{2}\sum_i hn_i + \frac{R}{k}\sum_i \frac{hn_i \exp(-hn_i/kT)}{[1-\exp(-hn_i/kT)]} \quad (\text{for} \quad Q_{\text{vib}} = \sum_i \frac{1}{[1-\exp(-hn_i/kT)]}) \tag{5}$$

where Q_{vib}, Q_{rot}, Q_{trans} are the partition function for E_{vib}, E_{rot} and E_{trans}. k is the Boltzmann's constant, h the Planck's constant, and v_i the individual vibrational frequencies, σ is symmetry number, I is moment of inertia, I_{A}, I_{B}, and I_{C} are moments of inertia of A, B, and C axes, M is the molecular weight. (E_{rot}(linear) and E_{rot}(nonlinear) are used for linear and nonlinear systems, respectively.)

The contributions to entropy S are provided by

$$S_{\text{tra}} = \frac{5}{2}R\ln T + \frac{3}{2}R\ln M - R\ln p - 2.31482 \tag{6}$$

$$S_{\text{rot}}(linear) = R\ln[\frac{8p^2IkT}{sh^2}] + R \tag{7}$$

$$S_{\text{rot}}(nonlinear) = \frac{R}{2}\ln[\frac{p}{\sqrt{s}}\frac{8p^2cl_A}{h}\frac{8p^2cl_B}{h}\frac{8p^2cl_C}{h}(\frac{kT}{hc})^3] + \frac{3}{2}R \tag{8}$$

$$S_{vib} = R\sum_i \frac{hn_i/kT\exp(-hn_i/kT)}{1-\exp(-hn_i/kT)} + R\sum_i \ln[1-\exp(-hn_i/kT)] \tag{9}$$

where the S_{vib}, S_{rot} and S_{trans} respectively represent the vibrational, rotational and translational contributions.

Gibbs energy can then be calculated with the equation

$$G = H - TS \tag{10}$$

Thermodynamic performance at different temperatures and electric intensities is calculated with the Dmol3 module. A macro-canonical ensemble (NVT) is selected for the calculations of all structures. Time step is set to 1.0 fs, and total simulation time of 0.01 ps is selected. The all-electron potential function is determined, and the electron wave function is performed with the double-number function with the *d* orbital.

The binding energy is calculated with the CASTEP module and the computational parameters are as follows. The electronic exchange-correlation energy is treated by the generalized gradient approximation method proposed by Perdew–Burke–Ernzerhof [14,15]. The convergence of the results with respect to energy cutoff and *k*-points [16] was carefully considered. A plane-wave basis set is utilized with an energy cutoff of 330 eV. Summation in the Brillouin zone for the bulk structures was performed with a Monkhorst-Pack *k*-point mesh [17] with 0.04 nm^{-1} spacing for all calculations. The tolerance values for geometry optimization in the CASTEP module are selected within the total energy of 5.0×10^{-6} eV/atom, maximum ionic Hellmann-Feynman force of 0.01 eV/Å, maximum ionic displacement of 5.0×10^{-4} Å, and maximum stress of 0.02 GPa.

Results and discussion

Crystal structures of the precipitates. The Al–Zn–Mg–Cu system is composed of age-hardening alloys arranged in a generally accepted typical precipitation order: supersaturated solid solution (SSS), Guinier–Preston (GP) zones, metastable phase η', and stable phase η [18-20]. Berg's study [18] pointed that the GP zone could be divided into GPI and GPII zones; each zone had a different arrangement of atom clusters. The GPI zone is coherent with the Al matrix and has an internal arrangement for the Zn and Al/Mg atoms on the $\{110\}_{Al}$ planes. The GPII zone contains a Zn-rich layer on the {111} planes of the Al matrix. This zone expands along the <110> direction of the Al lattice. Metastable phase η' is semi-coherent with the matrix, which has lattice parameters of $a = 0.496$ nm $\approx [211]/2_{Al}$ and $c = 1.40$ nm $\approx 2[111]_{Al}$ [21-23]. Stable phase η ($MgZn_2$ phase) is incoherent with the matrix and has a hexagonal structure with lattice parameters of $a = 0.5221$ nm and $c = 0.8567$ nm [24-27]. The GP zones, metastable phase η', and stable η ($MgZn_2$) phase, shown in Fig. 1, are constructed in this study to investigate the influence of the external electric field. GPI zone is constructed consisting of three aluminum matrix units to reflect the periodic structure of the precipitated phases and to reduce the amount of calculations [18]. GPII zone consists of four aluminum matrix units [18], and metastable phase η' and η ($MgZn_2$) phase consist of one unit cell each. For the uncertainty of structure of metastable phase η', we consider two of the most widely accepted structures at present, named as η'I [21] and η'II [22] (shown in Figs. 1(c) and 1(d)). The lattice parameters are shown in Table 1.

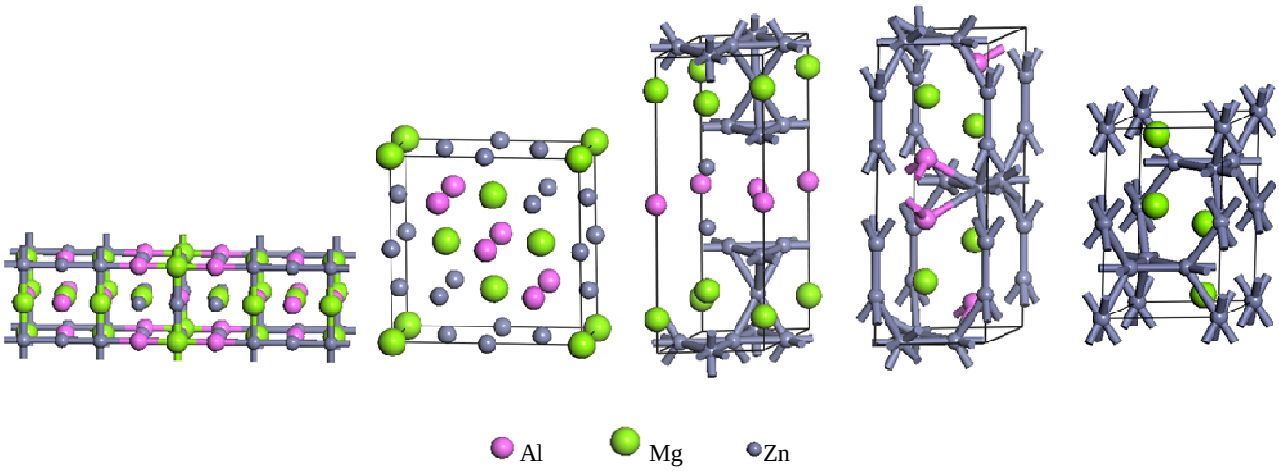

Fig. 1 Crystal structures of the calculated unit cells. (a) GPI,(b) GPII,(c,d) η' phase (η'I, η'II), (e) η phase.

Table 1. Lattice parameters of the calculated precipitates

Phases	**GPI**	**GPII**	**Al1Mg4Zn11(η'I phase)**	**Al4Mg4Zn10(η'II phase)**	**η' (Exp.)**	**$MgZn_2$(η)**	**$MgZn_2$(Exp.)**	**$MgZn_2$(Cal.)**
Cryst. Sys.	tetragonal	tetragonal	hexagonal	hexagonal		hexagonal		
Space Group	I4/mcm	I4/mcm	P-6m2	P-6		P63/mmc		
a(Å)	4.050	4.05	4.96 [21]	4.96 [22]	4.96 [21]	5.184	5.21 [24,25] 5.15 [26]	5.223 [27]
b(Å)	12.15	8.1	4.96 [21]	4.96 [22]	4.96 [21]	5.184	5.21 [24,25] 5.15 [26]	5.223 [27]
c(Å)	4.05	8.1	14.02 [21]	14.02 [22]	14.0 [21]	8.691	8.60 [24,25] 8.48 [26]	8.566 [27]
α(°)	90	90	90	90	90	90	90	
β(°)	90	90	90	90	90	90	90	
γ(°)	90	90	120	120	120	120	120	
V(Å^3)		265.7	298.7	298.7		202.3		202.4 [27]

Determination of stability. The binding energies per atom (E_b^P) of the GP zones, η' and η phases are calculated from the following equations [27]:

$$E_b^P = -\frac{1}{n_1+n_2+n_3}[E_t^P - n_1E_a^{Al} - n_2E_a^{Zn} - n_3E_a^{Mg}] \quad (11)$$

where E_t^P is the total energy at 0K, E_a^{Mg}, E_a^{Zn}, and E_a^{Al} are the energies per atom of the free Mg, Zn,

and Al atoms, respectively. The calculated energies per atom of the free Mg, Zn, and Al atoms are –972.51, –1708.67, and –52.87 eV, respectively. Consequently, the calculated binding energies per atom of the GPI, GPII, η' and η zones/phases are 1.587, 1.64, 1.76 and 3.244 eV/atom (153.05, 158.16, 169.73 and 312.85 kJ/mol, respectively).

Binding energy shows how strong or weak the atom combination is and marks the stability of the phase. The η phase has the largest binding energy in the former states. At appropriate thermodynamic and kinetic conditions, the GP zones may transform into the η phase, which has higher stability than the GP zones. This trend is consistent with the precipitation order of Al–Zn–Mg–Cu alloys during aging [18-20]. The tested differential scanning calorimetry (DSC) curve of quenched Al 7050 is shown in Fig. 2. Each phase transformation step is an exothermic process corresponding to the four exothermic peaks from 50 °C to 250 °C in the DSC curve. The four peaks correspond to the precipitations of GPI, GPII, metastable phase η', and stable phase η.

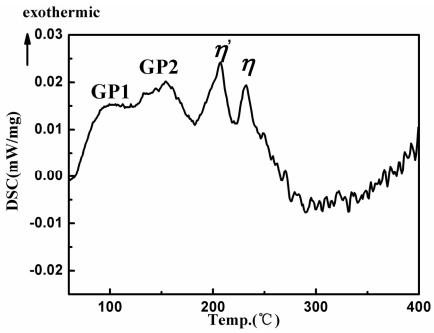

Fig. 2 DSC curve of quenched an Al-Zn-Mg-Cu alloy.

Effect of the external electric field intensity on aging phase transformation. Figs. 3(a) and (b) show the influence of the external electric field on the free energy of the GPI and GPII zones, which may precipitate firstly in the form of atom clusters in the Al–Zn–Mg–Cu alloys during aging treatment [18-20]. Fig. 3(a) show that the free energy of the GPI zone is insensitive to electric intensity. Thus, the formation or nucleation of the GPI zone cannot be accelerated by enhancing electric intensity. The GPII zone exhibits a similar response with GPI when electric intensity is lower than 31.2 MV/cm (shown in Fig. 3(b)). However, with electric intensity higher than 36.4 MV/cm, the free energy of the GPII zone drops. That is, if the external electric intensity is higher than 36.4 MV/cm, the formation or nucleation of the GPII zone can be accelerated. For η'I and η'II, with the external electric field intensity lower than 26 MV/cm, the free energy drops evidently, as shown in Fig. 3(c) and 3(d). Based on the change of free energy of η' phase and GP zones with electric field lower than 26 MV/cm, it can be concluded that the phase transformation from GP zones to η' phase can be promoted by the applied electric field. Along with the further increase of electric intensity, the free energy of η' phase instead increases (shown in Figs.3(c) and 3(d)). Combining the result of GP zones with that of η' phase, the phase transformation from GP zones to η' phase may be delayed with the applied electric field higher than 26 MV/cm. Fig. 3(e) shows that only with the electric field higher than 26 MV/cm can induce the decrease of η phase's free energy, which is the exact opposite of η' phase. As a result, with the electric intensity lower than 26 MV/cm, the phase transformation from η' phase to η phase may be delayed. When the

electric field higher than 26 MV/cm and lower than 52 MV/cm, the phase transformation from η' phase to η phase may be stimulated. As mentioned above, in order to gain optimal Al matrix with strengthening precipitate of η' phase [19,20], the external electric intensity should be lower than 26 MV/cm.

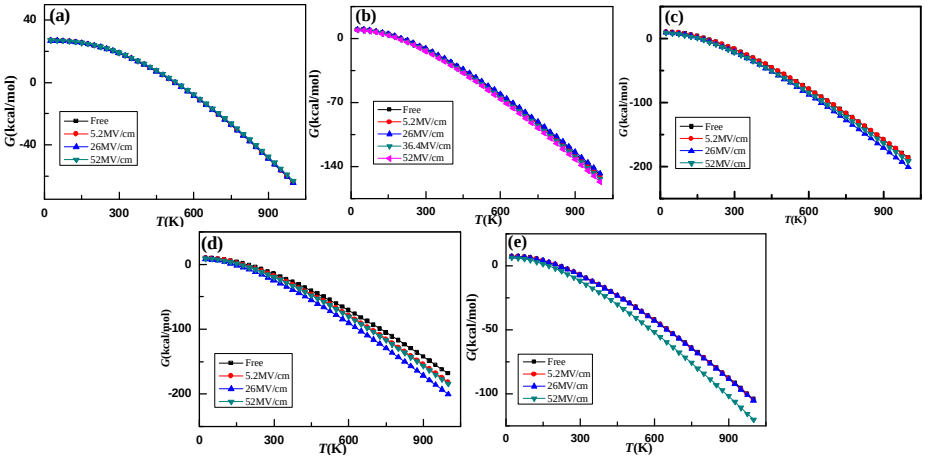

Fig. 3 Gibbs free energy of the different precipitates with different electric intensities along the z axis. (a) GPI, (b) GPII, (c) η'Ⅰphase, (d) η'Ⅱ phase, (e) η phase.

Lattice structures during phase transformations. The GPII zones are planar (111) sheets with high Zn content in Al matrix, and the (0001) and (11-20) planes of η' phase are always respectively parallel to the (111) and (110) planes of the Al matrix. Therefore, (111) plane of Al matrix (see Fig. 4(a)) is suitable to analyze the phase transformation between the GPII zone and η' phase. Fig. 4(b) shows the structural projection of the Al matrix with three layers along the <111> zone axis. When the Al atoms are replaced with Zn atoms, it will result in the formation of GPII zone. The adjacent atoms in the upper and under layers around one Zn atom in the middle layer will form the erected and inverted triangular bonds (see the diagram in Fig. 4(b)). For Zn has a smaller radius than Al, the spacing between the rows of atoms is approximately 6% to 8% less than that in the Al matrix. Given that the Zn atoms at the special positions in the middle layer of GP zone are replaced with Mg atom (comparing Fig.4(b) with Fig.4(c)), the unit of the transition structure between GPII and η' phase can be constructed. At the same time, the contraction of the interatomic distance in the upper and under layers in GPII is offset by the replaced Mg atoms in the middle layer for the larger size of Mg atoms than Zn and Al atoms. The representative structural projection of the η'Ⅰ , η'Ⅱ and η phases along the <0001> zone axis can be constructed like Figs. 4(c)-(e). And the (10–10) and (11–20) planes of them are shown in Figs. 4(f)-(k). In which, every two repeating units consisting of Zn atoms and interstitial Mg atoms are separated by one layer of Al atoms. Fig. 4(e) shows the atom distribution of the η phase along $<0001>_{\eta}$ zone axis. The inherited unit from the former η' to η phase are outlined in dotted frames. Between every five layers of repeating units, the main structure of η' phase shows one layer of Al atom. Once the Al atoms are replaced by Mg atoms, the transformation from η' phase to η phase may take place. Based on the analysis above, the diffusion of Mg atom plays a dominant role in the whole process of phase transformation. The calculations show that the un-bonded Mg atom is easily affected by the applied electric field and may break away from their original lattice sites under the action of electric field. And this migration

may directly affect phase transformations.

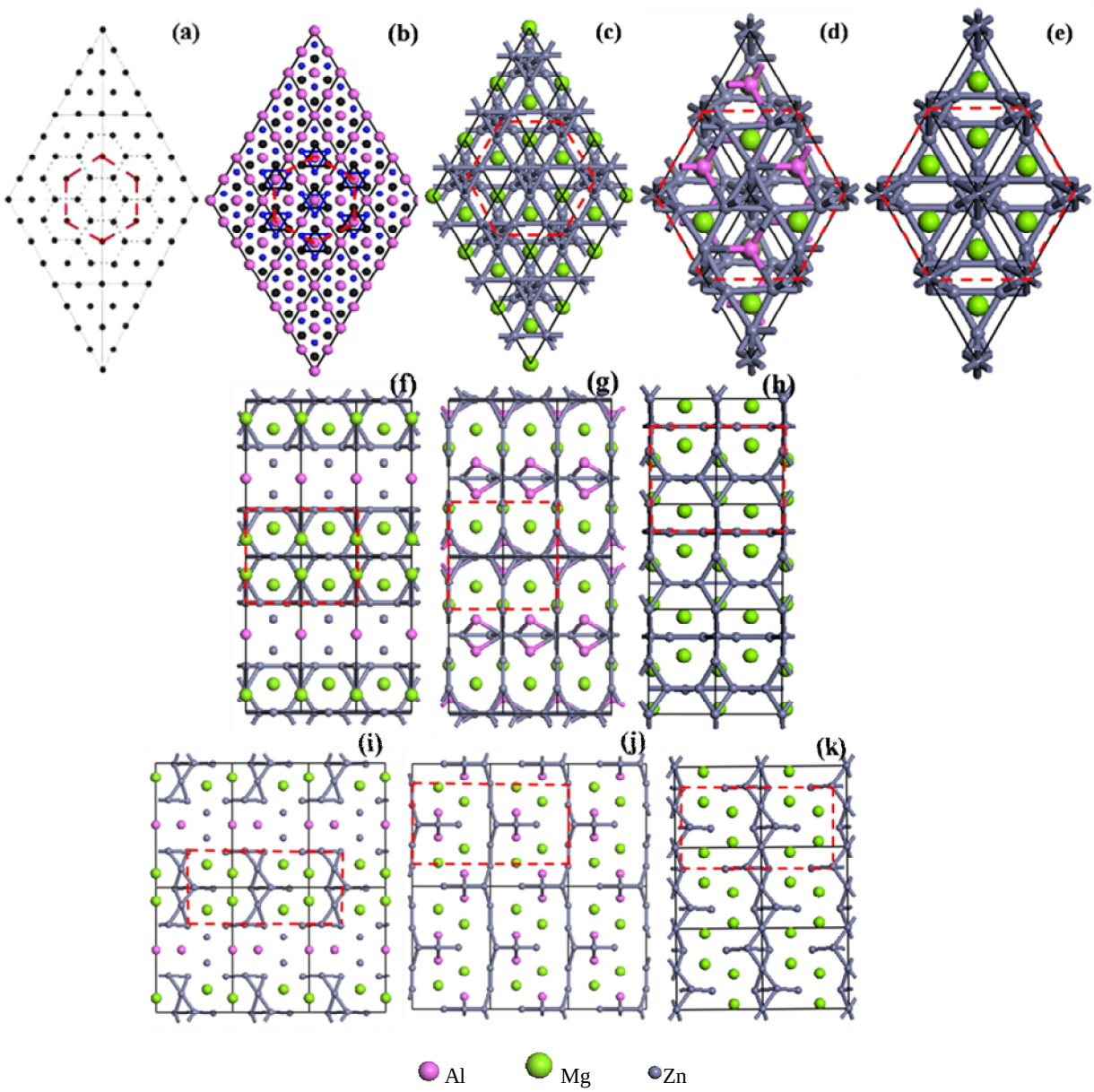

Fig. 4 Schematic of (a) atom distribution in the (111) plane of Al, (b) structural projection of the Al matrix with three layers along the $[111]_{Al}$ zone axis, (c) and (d) structural projection of the η' and η phases along the $[0001]_{\eta'}$ zone axis, (e),(f) and (g) atom distributions in the (10-10) plane of η'Ⅰ, η'Ⅱ and η phases, (h), (i) and (j) atom distributions in the (11-20) plane of η'Ⅰ, η'Ⅱ and η phases.

Conclusions

At the condition of aging with an applied electric field lower than 26MV/cm, phase transformation during aging in Al–Zn–Mg–Cu alloy from the GP zones to the η' phase may be accelerated, and the phase transformation from η' to η phase may be delayed, which is attributed to the different responses of these zones/phases to the external electric field. As a result, when aged in the presence of an electric field, the samples may achieve optimized microstructure.

Acknowledgment

This work was financially supported by the Fundamental Research Funds for the Central

Universities (XDJK2014C008 and SWU115068), the Chongqing scientific and technological projects (CSTC2014JCYJYS0001,CSTC2012GGYS0001), and by Program for the Youth Talent in Science and Technology of Chongqing(CSTC2014KJRC-QNRC50006).

References

1. E. Liotti, A. Lui, R. Vincent, S. Kumar, Z. Guo, T. Connolley, I.P. Dolbnya, M. Hart, L. Arnberg, R.H. Mathiesen and P.S. Grant: Acta Mater., Vol.70 (2014) No.15, p.228.
2. L. Li, Q.F. Zhu, Y.B. Zuo, C.Y. Ban, L.Z. He, H.T. Liu and J.Z. Cui: Mater. Charact., Vol.95 (2014), p.1.
3. J.Z. Wang, J.G. Qi, Z.F. Zhao, H.S. Guo, and T. Zhao: T. Nonferr. Metal Soc., Vol.23 (2013) No.9, p. 2792.
4. B. Liu, Z. Chen, Y.X. Wang and X.N. Wang: Mater. Sci. Eng. A, Vol.313 (2001) No.1-2, p. 69.
5. J.J. Zhang, Z. Chen, Y.X. Wang and B. Liu: J. Alloy Compd., Vol. 457 (2008) No.1-2, p. 526.
6. C.L. Zhang, P.D. Han, Z.X. Zhang, M.H. Dong, L.L. Zhang, X.Y. Gu, Y.Q. Yang and B.S. Xu: J. Mol. Model, Vol. 18 (2012) No. 3, p. 1123.
7. M.T. Baei, A.A. Peyghan, M. Moghimi and S. Hashemian: Superlattices Microstruct., Vol.52 (2012) No.6, p. 1119.
8. P. Hohenberg and W. Kohn: Phys. Rev. B, Vol.136 (1964) No.3B, p. 864.
9. D. Vanderbit: Phys. Rev. B, Vol.41 (1990) No.11-15, p. 7892.
10. M.D. Segall, P.J.D. Lindan, M.J. Probert, C.J. Pickard, P.J. Hasnip, S.J. Clark and M.C. Payne: J. Phys.: Condens. Matter, Vol.14 (2002) No.11, p. 2717.
11. B.J. Delley: Chem. Phys., Vol. 92 (1990) No.1, p. 508.
12. A. Putrino, D. Sebastiani and M. Parrinello: J. Chem. Phys., Vol.113 (2000) No.11, p.7102.
13. Z.W. Huang, Y.H. Zhao, H. Hou and P.D. Han: Physica. B, Vol.407 (2012) No.7, p.1075.
14. J.P. Perdew, J.A. Chevary, S.H. Vosko, K.A. Jackson, M.R. Pederson, D.J. Singh and C. Fiolhais: Phys. Rev. B, Vol.46 (1992) No.11-15, p.6671.
15. J.P. Perdew, K. Burke and M. Ernzerhof: Phys. Rev. Lett., Vol.77 (1996) No.18, p. 3865.
16. H.J. Monkhorst and J.D. Pack: Phys. Rev. B, Vol. 13 (1976) No.12, p.5188.
17. H. Monkhorst: Phys. Rev. B, Vol. 20 (1976) No.4, p. 1504.
18. L.K. Berg, J. GjΦnnes, V. Hansen, X.Z. Li, M. Knutson-wedel, G. Waterloo, D. Schryvers and L.R. Wallenberg: Acta Mater., Vol.19 (2001) No.17, p. 3443.
19. C.M. Li, Z.Q. Chen, S.M. Zeng, N.P. Cheng and T.X. Chen: Sci. China Tech. Sci., Vol. 56 (2013) No. 11, p. 2615.
20. X.B. Yang, J.H. Chen, J.Z. Liu, P. Liu, F. Qin, Y.L. Cheng and C.L. Wu: Mater. Charact., Vol. 83 (2013) p. 79.
21. J.H. Auld and S.M. Cousland: Scripta Metal., Vol. 5 (1974) No. 9, p. 194.
22. X.Z. Li, V. Hansen, J. GjØnnes and L.R. Wallenberg: Acta Mater., Vol.47 (1999) No.9, p. 2651.
23. S.P. Ringer and K. Hono: Mater. Charact., Vol. 44 (2000) No.1-2, p.101.
24. G. Wandahl and A.N. Christensen: Acta Chem. Scand., Vol. 41 (1987) No. 6, p. 358.
25. Y. Komura and K. Tokunaga: Acta Cryst., Vol. B36 (1980) No. 7, p.1548.
26. J.B. Friauf: Phys. Rev., Vol. 29 (1927) No. 1, p.34.
27. T.Ohba, Y. Kitano and Y. Komura, Acta Cryst., Vol. 40 (1984) No.1, p. 1.